Single-Layer, Multi-Mode OAM Reflectarray Antennas

Single-layer, Multi-Mode OAM Reflectarray Antennas

M. Beccaria, G. Dassano, P. Pirinoli

***Abstract*—In this letter, an innovative ReflectArray (RA) antenna able to radiate in the same direction multiple Orbital Angular Momentum (OAM) modes, is presented: depending on the direction of arrival of the impinging field, the RA radiates a broadside beam carrying on an OAM mode with different index. Two circular RAs with diameter $D = 19.8\lambda$ at the the frequency $f_0 = 30$ GHz, able to radiate two or four OAMs, have been designed and simulated, while a prototype of the dual-mode configuration has also been manufactured and experimentally characterised. The obtained results prove that vortex beams are successfully generated in the range of frequencies from 28 to 32 GHz, confirming the effectiveness of the proposed design.**

***Index Terms*—Reflectarray, Antennas, OAM.**

I. Introduction and Motivations

The next generation of wireless communication systems will require larger channel capabilities than those currently provided. This could be obtained *a)* moving the carrier frequency up to millimeter waves or either higher frequencies and *b)* enhancing the efficiency of the frequency spectrum by using proper multiplexing techniques. In alternative to more conventional approaches, recently the possibility to use Orbital Angular Momentum (OAM) – carrying beams is also investigated, since modes characterized by different index ℓ are orthogonal each others. Moreover, they radiate a conical beam, that could be useful in some applications [1].

The interest on the possibility to design antennas able to radiate OAM modes is therefore rapidly growing. Among the different proposed solutions, it is worth to mention spiral plates antennas [2] – [4], travelling-wave antennas [5], [6] and dielectric resonators [7]. Other configurations for the generation of OAM modes recently studied are those based on the use of transmitarrays [8] – [10], metasurfaces [11] – [15] or reflectarrays (RAs). Starting from [16], where preliminary numerical results on a perforated dielectric RA designed to radiate OAM mode with $\ell = +1$ are summarized, several papers on the design of RAs able to radiate single OAM modes have been published [17]- [22].

However, to obtain an efficient multiplexing scheme, it is necessary to radiate simultaneously more OAM modes, possibly in the same direction. While in [24], a configuration based on the use of two polarizations to realize a small size RA able to only radiate 2 OAM modes with indexes $\ell = \pm 2$ is introduced, other, more complex, solutions are presented in [23]- [27]: they consist in adopting four different feeds, two characterized by a x-polarization and the other twos by y-polarization, each illuminating a different area of the RA, and therefore responsible for the generation of a different OAM mode [23], in a composite structure including a transmitarray, a polarization rotated RA and a dual linear polarization horn [25], in the use of a folded RA including active elements [26] or in a multi-layer plasma reflectarray [27].

An alternative to design a simpler configuration can be that of using the superposition of the aperture field to generate different modes, i.e. implementing a principle similar to those already adopted in the design of bifocal RAs [28], [29]. This idea has already been proposed in [30]- [32], where the results on three different configurations based on this concept are designed: they radiate only two OAM modes in two different directions following a design procedure similar to that adopted for a bifocal RA, usually designed to provide a phase that is the mean value between those necessary to point the main beam in two different directions. Note that while the design of a bifocal RA essentially allows to change the pointing direction within those used for the reflectarray design, in the case of OAM if the phase is just given as a linear combination of those required for generating two specific modes, no other can be obtained. It means that the solutions proposed in [30]- [32] can just radiate the two modes for which they have been designed. In opposite to what done in bifocal design and in [30]- [32], here the principle of superposition is used to design a RA generating different OAMs that point all in the same (broadside) direction. While very preliminary numerical results on a two OAM RA were presented in [33], here to different configurations, supporting 2 or 4 modes are designed and numerically characterized; moreover, a prototype of the dual-mode reflectarray has been manufactured and experimentally characterized.

II. Reflectarray Design

To generate a beam carrying on an OAM mode, each element (i, j) of the reflectarray must provide a phase $\phi_{i,j}^{(\ell)}$ evaluated as [34]:

$$\phi_{i,j}^{(\ell)} = \frac{2\pi D_{i,j}}{\lambda_0} + \ell \times \arctan \frac{y_j}{x_i} \tag{1}$$

where, $D_{i,j}$ is the distance between the feed and the (i, j) element, λ_0 is the wavelength in the free space evaluated at the design frequency f_0, ℓ is the considered OAM mode index and (x_i, y_j) are the coordinates of the centre of the (i, j) element.

In the case in which the same aperture would be used to generate N OAM modes, ideally the RA must guarantee the phase distribution $\Phi^{(\ell_n)}$ required by each of them; however, if the unit-cell is characterized by only one degree of freedom, the RA can provide just a phase distribution, Φ_{mean}, that,

This paper was produced by the IEEE Publication Technology Group. They are in Piscataway, NJ.

Manuscript received April 19, 2021; revised August 16, 2021.

using the principle of superposition, can be written as a linear combination of the different $\Phi^{(\ell_n)}$

$$\Phi_{mean} = \frac{1}{N}\sum_{n=1}^{N}\Phi^{(\ell_n)} \tag{2}$$

In the examples considered here, $\Phi^{(\ell_n)}$ represents the phase distribution necessary to generate the OAM with index ℓ_n, pointing in the broadside direction, when the field radiated by the feed impinges on the reflecting surface with angles $(\theta_{\ell_n}^{inc}, \varphi_{\ell_n}^{inc})$.

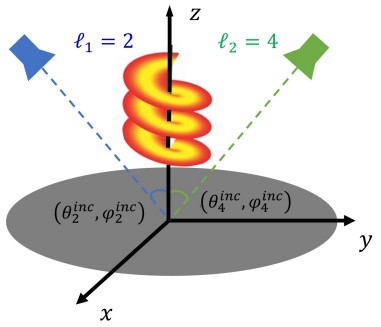

Fig. 1. Sketch of the reflectarray geometry generating 2 OAM modes.

For simplicity, let refer to the geometry sketched in Fig. 1, consisting in a circular reflectarray and two feed horns, located in two different positions and assume that two OAM modes with indices $\ell_1 = 2$ and $\ell_2 = 4$ would be obtained. When the feed identified by ℓ_1 is the only switched on, the direction of incidence is characterized by $(\theta_2^{inc} = 30°, \varphi_2^{inc} = 270°)$ and therefore the phase map $\Phi^{(2)}$ represented in the top left side of Fig. 2 is required to radiate the mode with index ℓ_1. Vice versa, when is the ℓ_2-feed to be switched on, a different RA must be designed, taking into account of the different direction of arrival of the incident field, characterized by $\theta_4^{inc} = 30°$ and $\varphi_4^{inc} = 90°$ and of the different mode ℓ_2 that would be generated: the required phase map $\Phi^{(4)}$ is that shown in the top right plot of Fig. 2.

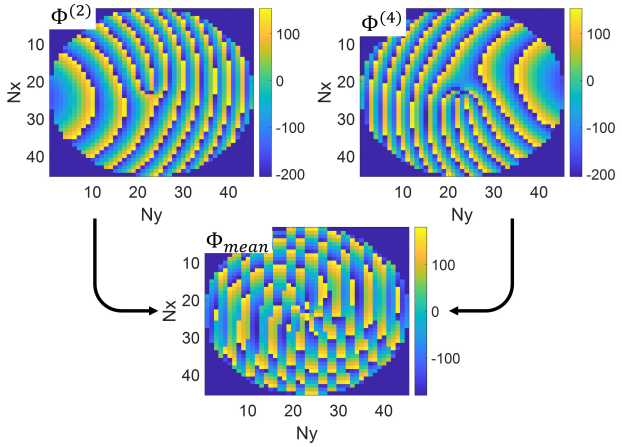

Fig. 2. Phase maps required for the generation of an OAM mode with $\ell = 2$ (top left), with $\ell = 4$ (top right) and for the dual-mode configuration (bottom).

Resorting to eq. 2 particularized for this case with $N = 2$, it is then possible to obtain the phase distribution Φ_{mean}, plotted on the bottom of Fig. 2, that must be provided by the RA. Note that the technique could be easily extended to a configuration generating a higher numbers of modes, simply increasing the number of feeds, located in different positions, evaluating all the $\Phi^{(\ell_n)}$ and finally computing Φ_{mean}. Since this is not the phase required to generate a single mode, it is reasonable to assume that each OAM will be a little distorted: however, the results in the next section will prove that the purity of the modes is just slightly affected by the not exact phase compensation and that the radiation patterns stay the same at least in the region of the main beam and nearby.

The proposed approach has been applied to the design of two circular reflectarrays, both with a diameter $D = 19.8\lambda_0$ at the design frequency $f_0 = 30\,\text{GHz}$. The RA surfaces are discretized with 1596 unit-cells. Each unit-cell has size equal to $0.45\lambda_0$ and consists in a square patch printed on a single layer Diclad 527 ($\epsilon_r = 2.55$, $\tan_\delta = 0.0022$) substrate, with a thickness $h = 0.8$ mm. Varying the side W of the patch it is possible to obtain a total variation of almost 280° for the phase of S_{11} [35] while its amplitude stays almost equal to 0 dB everywhere. The feed is the smooth-wall circular horn introduced in [36] located at a distance F from the planar surface, such that $F/D \approx 1$, in order to reduce the blockage and the spillover.

The first is a dual-mode RA, designed to provide the OAM modes with indices $\ell_1 = 2$ and $\ell_2 = 4$: the geometry is that shown in Fig. 1, while the phase map that the RA must provide is Φ_{mean} in Fig. 2. The second reflectarray is a quad-mode configuration, designed to radiate in addition to the OAMs 2 and 4 also those with indices $\ell_3 = -2$ and $\ell_4 = -4$; for their generation, two further feeds are needed, located at the same distance F from the planar surface, but in such positions that the directions of arrival of the incident field on the RA are characterized by $(\theta_{-2}^{inc} = 30°, \varphi_{-2}^{inc} = 180°)$ and $(\theta_{-4}^{inc} = 30°, \varphi_{-4}^{inc} = 0°)$.

III. Numerical and Experimental Results

To validate the design effectiveness, several tests have been done. First, the two designed antennas have been numerically analyzed with the full-wave approach of CST Microwave Studio, considering for both of them all the configurations for the generation of the different modes.

The field on a planar surface located in the near field region of the RAs (at 350 mm from their surface) has been computed, in order to check if the amplitude and phase distributions are those typical of the OAM mode with the considered index. The results relating to the dual-mode RA are shown in Fig. 3; on the top it is plotted the wavefront amplitude (left) and phase (right) distributions for the antenna configuration in which the feed is located in the position that guarantees angles of incidence $(\theta_2^{inc}, \varphi_2^{inc})$: as expected, in this case the waveform is that characteristic of the mode 2, while in the other case, when the direction of arrival of the incident field is identified by $(\theta_4^{inc}, \varphi_4^{inc})$ the field is clearly that associated to the OAM with index 4. As expected, the two modes are a little distorted, but for both of them, either the amplitude and the phase of the field are those typical of the considered OAM, and this confirms the possibility to use a structure like the designed one to generate more modes.

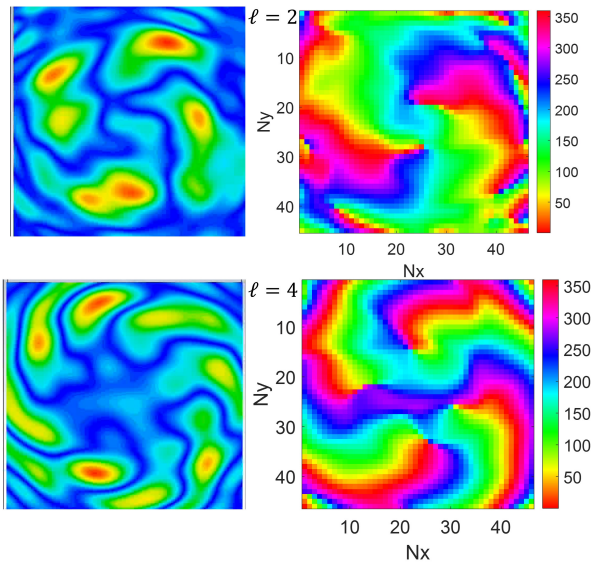

Fig. 3. Amplitude (left) and phase (right) distribution of the field associated to the OAM modes with indexes $\ell = 2$ (top) and $\ell = 4$ (bottom) evaluated on a plane at a distance of 350 mm from the dual-mode RA surface.

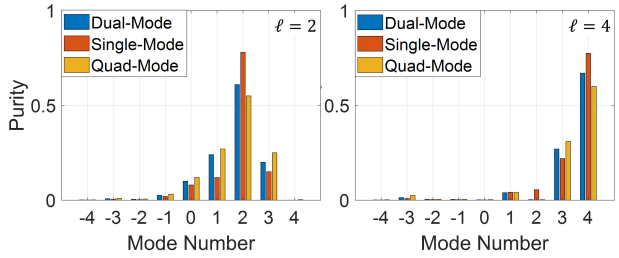

Fig. 4. Vortex spectrum expansion of the field radiated by single, dual- and quad-mode RAs and associated to the OAM modes with indexes $\ell = 2$ (left) and $\ell = 4$ (right).

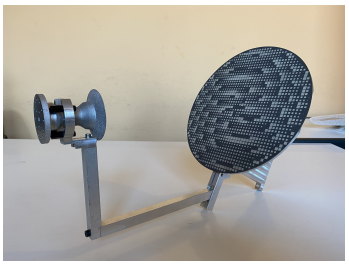

Fig. 5. Dual-mode RA prototype, with the feed oriented to generate the mode $\ell = 2$.

To verify the purity of each mode, the field radiated by both the RAs, when the position of the feed relative to the modes 2 and 4 are considered, has been expanded in terms of OAM modes, the energy W_ℓ associated to each mode has been evaluated and finally the ratio between W_ℓ and the total energy associated to the electric field, that can be written as

$$W_{tot} = \sum_{p=-\infty}^{+\infty} W_p \tag{3}$$

has been computed [26]. Note that, even if the sum in Eq. 3 runs from $-\infty$ to $+\infty$, in most of the practical cases it can be limited to the most significant modes. The vortex spectrum expansion relative to the two modes is represented in Fig. 4 for both the dual- and quad- mode RAs. In the same figure it is also plotted the spectrum composition of the field radiated by two single-mode RAs, designed to radiate the ℓ_1 or the ℓ_2 OAM mode, respectively. From the plots in Fig. 4 it clearly emerges that for the considered antennas the predominant mode is the desired one, even if the contribution of the mode 2 (or of the mode 4) slightly reduces moving from the single to the quad-mode configuration. Moreover, let consider for instance the histogram relating to the dual-mode RAs on the left (but similar consideration also applies to the histogram obtained for the quad-mode reflectarray or to the other plot): the predominant mode is that with index 2, plus some contributions from the OAM 1 and 3 but not from the fourth one, that is the other one radiated by the dual-mode RAs changing the feed position and this confirms the excellent decoupling between the modes.

In view of the promising numerical results, a prototype of the dual-mode reflectarray, shown in Fig. 5, has been manufactured and tested in the spherical near field test range in the anechoic chamber at Politecnico di Torino.

In the first two columns of Figs. 6-7 the numerical and experimental results obtained at 29, 30 and 31 GHz are reported. The results in Fig. 6 refer to the ℓ_1 mode, while the plots in Fig. 7 show the radiation patterns of the antenna configuration that generates the other OAM. As it can be seen, there is a very good agreement between the numerical and experimental results, being these last ones even better than those resulting from the RA simulations. This can be ascribed to the impossibility of imposing a very high accuracy in the discretization of the antenna model in order to keep under control the computational cost of the simulation, that is very high because the absence of any symmetry. The obtained patterns further confirm the effectiveness of the proposed design and also show that the main beam is quite stable over the entire frequency band. This observation is confirmed by the plot in Fig. 8, representing the variation of the measured gain with the frequency over a band ranging from 28 GHz up to 32 GHz, from which it appears that it stays quite stable over the entire frequency range. In the same plot it is also reported the gain for the two configurations evaluated at 29, 30 and 31 GHz, in very good agreement with the measured one.

In the right most column of Fig. 6 and of Fig. 7 the radiation pattern of the two single-mode antennas, obtained with their full-wave simulation, are also shown. As it can be seen, in both the cases the main lobe of the field radiated by the dual-mode or by the corresponding single-mode RA remains quite similar; clearly the not perfect phase compensation provided by the dual-mode configuration introduces phase error, and this corresponds to have some higher lobes out of the main beam region, and a decrease of the gain of almost 2.5 dB for both the analyzed modes, as it appears from Fig. 8, where the value of gain for the two single-mode RAs evaluated at 29, 30 and 31 GHz is also reported. This decreases of the gain is predictable, since it is an intrinsic consequence of the use of a single aperture for radiating the two modes and it is similar to what happens in bifocal configurations.

The radiation patterns in the H and E planes, obtained with the simulation of the single- dual- and quad-mode RAs and

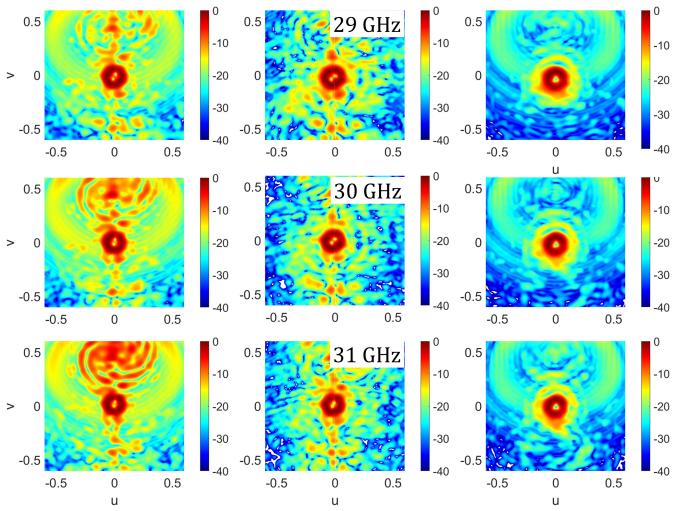

Fig. 6. Radiation patterns in the $(uv)-$plane at different frequencies for the mode $\ell = 2$. Dual-mode RA: numerical (left) and experimental (centre) results; single-mode RA: numerical results (right).

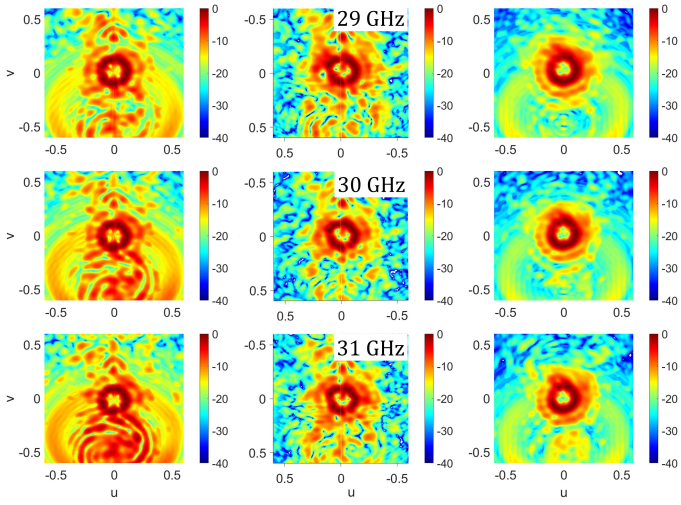

Fig. 7. Radiation patterns in the $(uv)-$plane at different frequencies for the mode $\ell = 4$. Dual-mode RA: numerical (left) and experimental (centre) results; single-mode RA: numerical results (right).

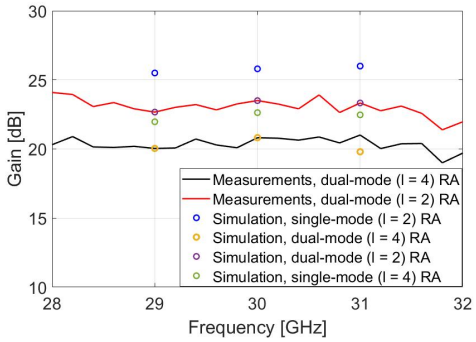

Fig. 8. Measured variation of the gain vs. frequency for both the modes 2 and 4 radiated by the dual-mode or single-mode RA.

the measurement of the dual-mode prototype, considering for all of them the configuration in which they radiate the mode 2, are finally shown in Fig. 9. They also confirm the feasibility of the multi-mode RA, since the radiation patterns are almost the same independently from the antenna, and the only effect of the presence of more modes is the already mentioned increase of the side lobes in the E-plane. If compared with the solutions proposed in [30]- [32], the proposed antennas presented the advantages to be able of radiating several modes, all in the same direction. For what concerns other parameters, as gain, efficiency and bandwidth, few results are available in literature. Referring to those summarized in table I of [32], it is possible to notice that the here proposed dual-mode RA has higher gain and better aperture efficiency. The bandwidth cannot be computed since the gain varies of less then 1 dB with respect to the value at f_0 for frequencies below 31.6 GHz, but probably it will satisfy this constrains also for frequencies below the lower considered limit of 28 GHz. Taking into account that maximising the bandwidth is not the aim of this work, and that a very simple re-radiating element is used, this is a good result.

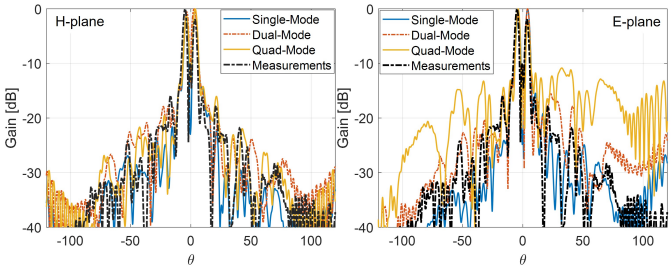

Fig. 9. Radiation patterns in the H (left) and E (right) planes for the mode 2, obtained with the simulation of the single-, dual- and quad-mode RAs and with the experimental characterization of the dual-mode prototype.

TABLE I
COMPARISON OF THE PROPOSED AND REPORTED OAM MULTI-MODE PERFORMANCE RA

Freq. [GHz]	SLL, E-plane [°] opt.feed	SLL, E-plane [°] "max eff." feed	SLL, H-plane [°] opt. feed	SLL, H-plane [°] "max eff." feed	Efficiency [%] opt. feed	Efficiency [%] "max eff." feed
29	-11	-9	-19	-16.6	44.87	43.15
30	-17.7	-15.5	-23	-18	51.7	49.5
31	-12.8	-10	-25	-19	48.66	46.37

IV. CONCLUSIONS

In this letter, an innovative single-layer passive Reflectarray, designed to radiate in the same direction several OAM modes is discussed. The results of the numerical analysis of two

TABLE II
COMPARISON OF THE PROPOSED AND REPORTED OAM MULTI-MODE PERFORMANCE RA.

	[30]	[31]	[32]	**This Work**
f_0	15 GHz	5.8 GHz	6 GHz	**30 GHz**
Apert. Area	$56.25\lambda^2$	$100\lambda^2$	$225\lambda^2$	$\mathbf{307.9\lambda^2}$
Polariz.	CP	LP	CP	**LP**
Anal. Mode	$l = +2$ $l = +1$	$l = +2$ $l = +1$	$l = \pm 1$	$\boldsymbol{l = +2}$ $\boldsymbol{l = +4}$
Dir. of Rad.	$\theta_{+2} = -30°$ $\theta_{+1} = +30°$	$\theta_{+2} = -30°$ $\theta_{+1} = +30°$	$\theta_{+1} = +20°$ $\theta_{-1} = -20°$	$\boldsymbol{\theta_2 = 0°}$ $\boldsymbol{\theta_{+4} = 0°}$
Max. Gain	17 dBi	14.7 dBi	22.2 dBic	**24 dBi**

different antennas, designed to generate 2 or for modes and the experimental characterization of a prototype of the dual-mode configuration confirm the effectiveness of the proposed solution and show that the features of the generated beams are comparable to those obtained using single-mode antennas.

REFERENCES

[1] M. Veysi, C. Guclu, F. Capolino and Y. Rahmat-Samii, "Revisiting Orbital Angular Momentum Beams: Fundamentals, Reflectarray Generation, and Novel Antenna Applications," IEEE Antennas Propag. Magazine, vol. 60, no. 2, pp. 68-81, 2018.

[2] G. A. Turnbull, D. A. Robertson, G. M. Smith, L. Allen and M. J. Padgett, "The generation of free-space Laguerre-Gaussian modes at millimeter-wave frequencies by use of a spiral phaseplate," Opt. Commun., vol. 127, no. 4, pp. 183-188, 1996.

[3] D. Zelenchuk and V. Fusco, "Split-ring FSS spiral phase plate," IEEE Antennas Wireless Propag. Lett., vol. 12, pp. 284-287, 2013.

[4] X. N. Hui et al., "Ultralow reflectivity spiral phase plate for generation of millimeter-wave OAM beam", IEEE Antennas Wireless Propag. Lett., vol. 14, pp. 966-969, 2015.

[5] S. Zheng, X. Hui, X. Jin, H. Chi and X. Zhang, "Transmission characteristics of a twisted radio wave based on circular traveling-wave antenna," IEEE Trans. Antennas Propag., vol. 63, no. 4, pp. 1530-1536, 2015.

[6] Z. Zhang, S. Zheng, X. Jin, H. Chi and X. Zhang, "Generation of plane spiral OAM waves using traveling-wave circular slot antenna," IEEE Antennas Wireless Propag. Lett., vol. 16, pp. 8-11, 2017.

[7] J. Ren and K. W. Leung, "Generation of microwave orbital angular momentum states using hemispherical dielectric resonator antenna," Appl. Phys. Lett., vol. 112, 2018.

[8] P. Feng, S. Qu and S. Yang, "OAM-Generating Transmitarray Antenna With Circular Phased Array Antenna Feed," IEEE Trans. Antennas Propag., vol. 68, no. 6, pp. 4540-4548, 2020.

[9] G. -B. Wu, K. F. Chan, K.M. Shum and C.H. Chan, "Millimeter-Wave Holographic Flat Lens Antenna for Orbital Angular Momentum Multiplexing," IEEE Trans. Antennas Propag., vol. 69, no. 8, pp. 4289-4303, 2021.

[10] F. Qin, R. Song, W. Cheng and H. Zhang, "Multibeam OAM Transmitarray With Stable Vortex Property Based on Bifocal Method," IEEE Antennas Wireless Propag. Lett., vol. 20, no. 9, pp. 1601-1605, 2021.

[11] L. -J. Yang, S. Sun, W. E. I. Sha, Z. Huang and J. Hu, "Arbitrary Vortex Beam Synthesis with Donut-Shaped Metasurface," IEEE Trans. Antennas Propag., vol. 70, no. 1, pp. 573-584, 2021.

[12] H. Lv, Q. Huang, X. Yi, J. Hou and X. Shi, "Low-Profile Transmitting Metasurface Using Single Dielectric Substrate for OAM Generation," IEEE Antennas Wireless Propag. Lett., vol. 19, no. 5, pp. 881-885, 2020.

[13] S. Iqbal, M.R. Akram, M. Furqan, H.A. Madni, M.I. Khan and G. Shu, "Broadband and High-Efficiency Manipulation of Transmitted Vortex Beams via Ultra-Thin Multi-Bit Transmission Type Coding Metasurfaces," IEEE Access, vol. 8, pp. 197982-197991, 2020.

[14] H. Liu, H. Xue, Y. Liu, Q. Feng and L. Li, "Generation of High-Order Bessel Orbital Angular Momentum Vortex Beam Using a Single-Layer Reflective Metasurface," IEEE Access, vol. 8, pp. 126504-126510, 2020.

[15] Z. Wang, X. Pan, F. Yang, S. Xu, M. Li and D. Su, "Design, Analysis, and Experiment on High-Performance Orbital Angular Momentum Beam Based on 1-Bit Programmable Metasurface," IEEE Access, vol. 9, pp. 18585-18596, 2021.

[16] X. Bai et al., "Perforated dielectric antenna reflectarray for OAM generation," IEEE Int. Symposium Antennas Propag. & USNC/URSI Nat. Radio Scie. Meeting, Vancouver, BC, Canada, 2015, pp. 2159-2160.

[17] H. Huang and S. Li, "High-Efficiency Planar Reflectarray With Small-Size for OAM Generation at Microwave Range," IEEE Antennas Wireless Propag. Lett., vol. 18, no. 3, pp. 432-436, 2019.

[18] Z. Akram et al., "Wideband Vortex Beam Reflectarray Design Using Quarter-Wavelength Element," IEEE Antennas Wireless Propag. Lett., vol. 18, no. 7, pp. 1458-1462, 2019.

[19] B. Li, P. F. Jing, L. Q. Sun, K. W. Leung and X. Lv, "3D Printed OAM Reflectarray Using Half-Wavelength Rectangular Dielectric Element," IEEE Access, vol. 8, pp. 142892-142899, 2020.

[20] Z. -Y. Yu, Y. -H. Zhang and H. -T. Gao, "A High-Efficiency and Broadband Folded Reflectarray Based on an Anisotropic Metasurface for Generating Orbital Angular Momentum Vortex Beams," IEEE Access, vol. 9, pp. 87360-87369, 2021.

[21] Y. Huang, X. Li, Z. Akram, H. Zhu and Z. Qi, "Generation of Millimeter-Wave Nondiffracting Airy OAM Beam Using a Single-Layer Hexagonal Lattice Reflectarray," IEEE Antennas Wireless Propag. Lett., vol. 20, no. 6, pp. 1093-1097, 2021.

[22] F. Li et al., "Generation and Focusing of Orbital Angular Momentum Based on Polarized Reflectarray at Microwave Frequency," IEEE Trans. Microw. Theory Tech., vol. 69, no. 3, pp. 1829-1837, 2021.

[23] X. Y. Lei and Y. J. Cheng, "Orbital angular momentum reflectarray antenna with multiple modes," Int. Workshop on Antenna Tech.: Small Antennas, Innovative Structures, and Applications (iWAT), Athens, Greece, 2017, pp. 316-318.

[24] Y. Chen, Y. Zhou, H. Jiang, H. Wang and H. Yang, "Wideband Dual-Polarized Vortex Beams Reflectarray Antenna with Independently Controllable Dual Modes," IEEE 4th Int. Conf. on Elect. Inf. and Comm. Tech. (ICEICT), Xi'an, China, 2021, pp. 207-210.

[25] P. K. Li, C. J. You, H. F. Yu, Q. Wang and Y. J. Cheng, "Dual Orbital Angular Momentum Mode Antenna by Combination of Transmitarray and Reflectarray," IEEE Int. Symposium Antennas Propag. & USNC/URSI National Radio Scie. Meeting, San Diego, CA, USA, 2017, pp. 1193-1194.

[26] B. Liu, S. -W. Wong, K. W. Tam, X. Zhang and Y. Li, "Multifunctional Orbital Angular Momentum Generator with High-Gain Low-Profile Broadband and Programmable Characteristics," IEEE Trans. Antennas Propag., vol. 70, no. 2, pp. 1068-1076, 2022.

[27] E. Koohkan, S. Jarchi, A. Ghorbani and M. Bod, "Vortex Beam Generation Based on Plasma Reflect-Array Surface at Microwave Frequencies," IEEE Trans. Plasma Science, vol. 49, no. 7, pp. 2086-2092, 2021.

[28] P. Nayeri, F. Yang and A. Z. Elsherbeni, "Bifocal Design and Aperture Phase Optimizations of Reflectarray Antennas for Wide-Angle Beam Scanning Performance," IEEE Trans. Antennas Propag., vol. 61, no. 9, pp. 4588-4597, 2013.

[29] G. -B. Wu, S. -W. Qu and S. Yang, "Wide-Angle Beam-Scanning Reflectarray With Mechanical Steering," IEEE Trans. Antennas Propag., vol. 66, no. 1, pp. 172-181, 2018.

[30] S. Yu et al., "Generating multiple orbital angular momentum vortex beams using a metasurface in radio frequency domain," Appl. Phys. Lett., vol. 108, 2016.

[31] M. Karimipour, N. Komjani, and I. Aryanian, "Holographic-inspired multiple circularly polarized vortex-beam generation with flexible topological charges and beam directions," Phys. Rev. Appl., vol. 11, no. 5, 2019.

[32] L. Yu, X. Li, Z. Qi, H. Zhu, Y. Huang and Z. Akram, "Wideband Circularly Polarized Dual-Mode Vortex Beams Reflectarray Design Using Dual-Semi-Split-Loop Elements," IEEE Antennas Wireless Propag. Lett., vol. 18, no. 12, pp. 2676-2680, 2019.

[33] M. Beccaria and P. Pirinoli, "Single layer Multimodal OAM Reflectarray," 16th Europ. Conf. on Antennas Propag. (EuCAP), Madrid, Spain, 2022, pp. 1-4.

[34] L. Yu and Y. J. Cheng, "High-Efficiency and High-Polarization Separation Reflectarray Element for OAM-Folded Antenna Application," IEEE Antennas Wireless Propag. Lett., vol. 16, pp. 1357-1360, 2016.

[35] M. Beccaria, P. Pirinoli and M. Orefice, "Numerical and Experimental Analysis of Convex Reflectarray Antennas," IEEE Int. Symposium Antennas Propag. & USNC/URSI National Radio Scie. Meeting, Fajardo, PR, USA, 2016, pp. 1419- 1420.

[36] Beccaria M, Addamo G, Orefice M, Peverini O, Manfredi D, Calignano F, Virone G and P. Pirinoli, "Enhanced Efficiency and Reduced Side Lobe Level Convex Conformal Reflectarray," Applied Sciences 11, no. 21: 9893, 2021.